Density functional LCAO calculations of vibrational modes and phonon density of states in the strained single-layer phosphorene

Krzysztof Pyrchla[a] and Robert Bogdanowicz[a,z]

[a] Department of Metrology and Optoelectronics, Faculty of Electronics, Telecommunications and Informatics, Gdańsk University of Technology, 11/12 Narutowicza St., 80-233 Gdańsk (Poland)

[z] Corresponding author: tel. +483471503, fax. +483471848, email: rbogdan@eti.pg.edu.pl (R. Bogdanowicz)

Abstract. The paper presents an investigation of phosphorene under axial strain on the phonon density of states and vibrational modes. The studies were performed by means of density functional theory (DFT) within the linear combination of atomic orbitals (LCAO). The strained models were constructed using optimised supercell techniques. The vibrational mode spectra were estimated for strains applied for both the zigzag and armchair directions of phosphorene. This approach is an attractive candidate for the calculation the dynamical matrix of the system because its numerical complexity gradually increases together with the size of the analysed cell. The shift of peaks in the PDOS of black phosphorene is monotonic, and inversely proportional to the applied strain over the zigzag direction. This relation is valid for small strains (below 10%) of peaks corresponding to modes B_{2g} and A_g^2. For a strain applied over the armchair PDOS, the shifts are proportional to the strain. The peak shifts tend to become higher as the strain increases. This dependence is not monotonic, and is clearly more rapid for compressing strains. Moreover, the peaks shift slower for an armchair strain than for a zigzag strain, revealing its strong anisotropy.

Introduction

In the past years, the rediscovering of materials which were known from a long time became a regular occurrence in nanotechnology. A good example of such a process is phosphorene. Phosphorus as a pure element is known from 1669, while black phosphorus, an allotrope form of bulk phosphorus, was synthesised in 1914 [1]. Despite the time that has passed since its discovery, these materials do not attract any special scientific attention until recently [2]. Their high toxicity, low band gap, and environmental instability [3] are without a doubt some of the reasons. The mentioned rediscovery is connected with the first synthesis of a few layers to a single layer of black phosphorus－Phosphorene [1,3,4].

Phosphorene, as a monatomic single layer crystal, is quite a unique material, but it excites the scientific community manly due to its properties [3,4]. Contrary to the first monatomic single layer material, Graphene, it is a semiconductor [5]. Similarly to other 2D materials such as graphene, molybdenum disulfide, and transition metal dichalcogenide (TMDC), its properties change when disassembled to single layer [1]. Unlike the other single layer semiconductors, such as MoS_2 and WS_2, the phosphorene band gap does not change its type when it is transformed from a bulk structure down to a single layer [1]. This is a crucial feature for future applications because few-layer structures are much easier to fabricate than single-layer ones.

As was described, pure phosphorene is unstable under environmental conditions, however, this material remains quite new. For these reasons, *ab-initio* methods had, and still have, an important role in research on phosphorene [6–8]. As this material is primarily being considered for optoelectronic applications, its electron band structure has been extensively studied [9]. The results from the beginning have shown that phosphorene's band structure is anisotropic. As a result, the effective carrier mass and its mobility differ between directions in phosphorene [10]. In the pure, relaxed material, the armchair direction is preferred for current flow because of the higher carrier mobility, however this kind of anisotropy could be challenging in technical applications. It was shown by first principles analysis that the direction of the preferred current flow can be modulated by arsenic doping [8]. Two-dimensional materials generally have a larger surface-to-volume ratio than bulk materials, and for this reason, the adsorption of adatoms on the surface is an effective way to change its properties.

Phosphorene is not only a unique 2D crystal because of its monatomic build. Its unusual properties are rooted in its layer anisotropy [10–12]. Despite this material's layers being monatomic, they have a different geometry in the armchair direction (puckers), and zigzag

2

direction (closely connected chains). Because of this structural geometry, many important mechanical properties are anisotropic. DFT *ab-initio* studies shows that the Young modulus, Poisson coefficient, and critical strain are angle-dependent [13]. Because of the anisotropy in the structure, and the bond energies, the phonon dispersion relations are also anisotropic [11]. As a result, the heat transport in phosphorene depends on the direction. The carrier transport properties are anisotropic in a similar way. Differences in charge mobility between directions where reported from the very beginning of phosphorene research [10]. A study of the dependences between the dispersion reaction in phosphorene can be find in [12].

Great attention has been paid to investigation of the strain properties of 2D materials, and phosphorene is no exception. Phosphorene has great durability for strain [14], which, in connection with its anisotropy, makes it a great candidate for strain engineering. It was reported that its electron band structure depends on the applied strain. Both the conduction and valence bands can change its shape in the specific Brillouin zone depending on stress tensor [15]. As an effect, the band gap changes its character from direct when phosphorene is unstrained to indirect under specific strains. The width of the band structure also changes with the applied strain [16]. This phenomenon creates the opportunity for some strain engineering features in phosphorene. Under both compressing and tensile strain, it is possible to transfer phosphorene from a semiconducting to a metallic state [17] for strains higher than 10%. Despite this, the application of a 6% strain could change the direction of the preferred conductance; rotating it by 90 degrees [10].

It is not only the electronic properties of phosphorene are affected by its unusual band structure behaviour. Its optical properties are also quite unique. Complex ab-initio research on the influence of light shows that strain can induce optical activity in this material [18].

The effective tool for in-situ measurements on 2D structures is Raman spectroscopy [19]. This kind of measurements became a standard method for measuring the properties of two-dimensional crystals. It is sensitive even to small changes in structure, which is important because strain affects many important properties of phosphorene, so a method of estimating the strain tensor in its structure is required.

The Raman spectra of strained phosphorene has been calculated many times using ab-initio approaches [20–22]. Some experimental works show that estimation of the strain tensor is possible under real conditions, using Raman spectroscopy [23].

3

The other question can arise about how the number of layers of phosphorene structure affects its Raman spectrum. According to exiting experimental data [24,25], the changes in the position of the Raman peaks indicated by changing the number of structure layers from 1 to 5 are below 3 cm^{-1} and the effect applies mainly to the peek A^2_g. Akhtar at al. [23] assigned corresponding Raman peaks of layered BP positioned at 360, 440, and 468 cm^{-1}. Furthermore, the other work of Akhtar [25] summarise that larger number of BP layers (2L to 5L) results rather in the Raman bands intensity increase than in their shift vs frequency.

Next, Lu et al. [24] reported thinning of phosphorene flakes by use of Ar-based plasma manifesting that thinning of few-layers phosphorene results in the A^2_g mode shift from 467.7 cm^{-1} (bulk BP) to 470 cm^{-1} (bilayer phosphorene).

Raman spectrum ab-initio simulations are still challenging. The level of theory used in the calculations differs significantly between authors. In some works, the calculations were performed using the plane-wave DFT method [21,26]. Other material science codes like CRYSTAL allows using of LCAO approach only for frozen-phonon calculation [27].

Even a simple LDA (local density approximation) functional can be used to calculate the vibrational modes [21], but it will lack a description of the long-range interaction, and tends to overestimate the bond strength, so it fails to describe the degeneracy of some modes [27]. To solve this problem, it was proposed to use hybrid functionals which, contrary to GGA or LDA functionals, can describe long-range interaction [27].

In the case of the LCAO method, the type of basis-set used in the calculation is crucial both for GGA or hybrid approximations. In work [28], the problem of basis-set optimization was raised. Due to the previously reported issues, the thoroughly optimized basis sets were applied in LCAO approach in this work. The details can be found in the supplementary information of the work [29].

In this work, a study of the usage of LCAO (linear combination of atomic orbitals) to estimate the PDOS (phonon density of states) and vibrational modes of phosphorene was presented. The vibrational properties of phosphorene were described in the literature [21,23,30] using *ab-initio* calculations, but mainly using the DFT plane-wave approach. To the best of our knowledge, there have been no attempts at a complex analysis of this process using DFT LCAO. In the paper, only axial strains are discussed. These strains are particularly crucial for the nanoengineering of phosphorene, because of its significantly different mechanical properties in different directions [31]. In this research, focus was put on strains being applied to the armchair

4

and zigzag axes. The DFT LCAO method was used as implemented in the ATK Quantumwise toolbox [32]. Applied approach is a promising candidate for calculation of the dynamic matrix of the system because the LCAO method in SIESTA implementation has linear scaling complexity O(N) [33]. This feature is particularly important because the standard method of computation performed in this work requires 2N times of electron density operations (N number of atoms in the system) to produce system dynamical matrix. Thus, the linear scaling complexity extending the maximal size of a cell could be used in these calculations.

1. Experimental

The model of the structure needed for the simulations was created using the Atomistix ToolKit Quantumwise (ATK, Synopsys, USA) [32]. The phosphorene structure used in the experiments was based on the black phosphorus structure, which is available in the ATK database. The structure geometry was optimised to remove any residual stresses which can arise in the structure in the transition from bulk to slab configuration. For force optimisation, the Broyden-Fletcher-Goldfarb-Shanno (LBFGS) algorithm was used. The procedure continues until the maximal force per atom falls below the truncation level, which was set to 10^{-4} eV/A.

For the calculation of the atomic interactions, the density functional theory (DFT) as implemented in the linear combination of atomic orbitals (LCAO) method [33] was applied. This method is included in the ATK package. The crucial feature of the LCAO approach is that its computational complexity depends linearly on the number of atoms in the system. The gradual increase in the complexity of the calculation is particularly important in dynamical matrix calculations. To solve the matrix equations of the LCAO method, self-consistent field (SCF) iterations were performed. During DFT calculation, the exchange-correlation of electrons was included using GGA method witch PBE (Perdew, Burke and Ernzerhof) functionals. Two types of calculations were conducted. To ensure that each calculation is converged, the tests were performed both for the k-points grid, and the energy of mesh cut-off. During geometry optimisation, the SG15 pseudopotential with medium basis set was utilised. The used basis set was developed basing on FHI-aims basis sets. The description of how these sets were created can be found in the appendixes of the article [29]. The SG15 is the norm-conserving pseudopotential with multiple projectors, semi-core states, and non-linear core correction implemented natively in the ATK software. The description of the procedure of generation of this pseudopotentials is described in the article [34]. For these calculations,

5

the k-points where set to 9x9x1 (Monkhorst-Pack). The mesh cut-off energy was set to 60 Ha. To improve the description of the Van der Waals interaction, it was decided to use the GrimmeDFTD3 correction, as described in [35]. It enables us to achieve closer to experimental interlayer spacing after the optimisation.

For the calculation of the dynamical matrix of the system, the different numerical parameters were utilized. The k-points were set to 31x21x1 (Monkhorst-Pack), and the mesh cut-off energy was set to 150 Ha.

The tolerance was set to 10^{-4} Ha for both calculations. This value should be understood as the maximal difference between the Hamiltonian matrix elements in successive, self-consistent steps.

A group of structures was made, which differed in their degree of defectiveness by strain. Strain is defined by the equation in (**1**).

$$\varepsilon_x = \frac{a_x - a_{x0}}{a_{x0}} \tag{1}$$

Where a_x denotes the length of the cell along the x axis after applying strain in this direction, and a_{x0} denotes the unstrained length of the cell in this direction.

The strains along the two specific directions of the phosphorene－armchair and zigzag－were studied. The strain values applied to the models were [-16, -12, -6, 0, 6, 12, 16] %. Each structure geometry, after the strain was applied, was optimized (see **Figure 1**). Because of the Poisson effect, the dimension perpendicular to the direction of the strain was set to be unconstraint. The implementation of LBFGS available in the ATK package allow the calculation to be performed under such conditions. During the optimisation process, the atoms' fractional coordinates and the length of the cell dimension perpendicular to the strain axis where optimised.

To calculate the Phonon density of states (PODS) for the studied nanostructure, the tetrahedron method [36] was applied. Integration of the reciprocal space, for the purpose of this method, was performed using the proper ATK calculator.

The vibrational modes of the structure were calculated as the eigenvalues of the dynamical matrix. Results postprocessing, selection, and plotting were performed in the MATLAB program.
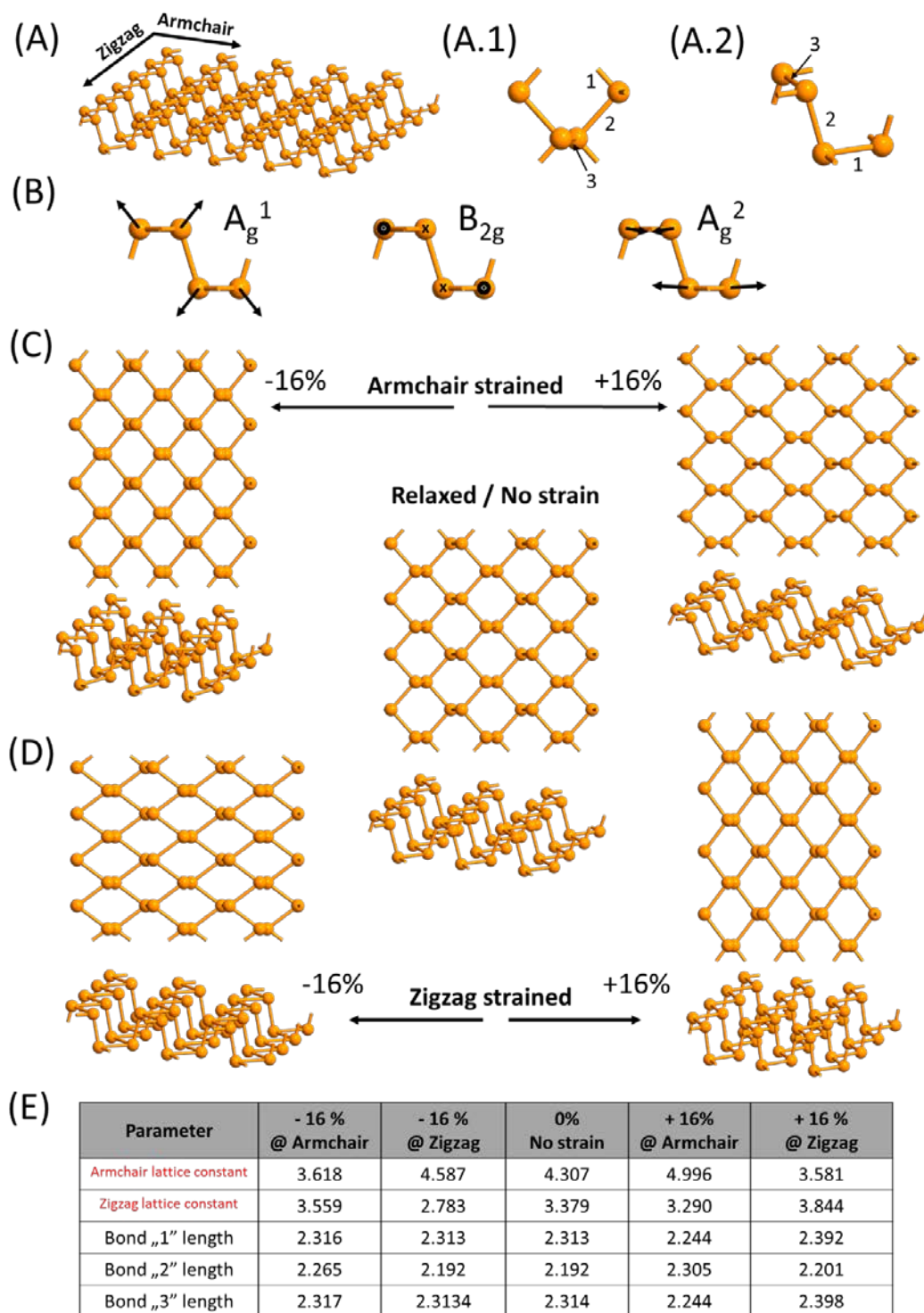
Figure 1. (A) A single layer phosphorene structure model with axes names and studied cell with marked bonds; (B) vibrational modes of a black phosphorus nanosheet where the arrows show the direction of movement of the atoms; (C and D) strained slabs in the zigzag and armchair directions +16%, -16%; (E) Dimensions of studied BP atomic structures. Attn. relaxed BP cell was shown as reference.

Parameter	- 16 % @ Armchair	- 16 % @ Zigzag	0% No strain	+ 16 % @ Armchair	+ 16 % @ Zigzag
Armchair lattice constant	3.618	4.587	4.307	4.996	3.581
Zigzag lattice constant	3.559	2.783	3.379	3.290	3.844
Bond „1" length	2.316	2.313	2.313	2.244	2.392
Bond „2" length	2.265	2.192	2.192	2.305	2.201
Bond „3" length	2.317	2.3134	2.314	2.244	2.398

2. Results and Discussion

2.1. Atomic structure model

The model of the structure used in the calculations had 4 phosphorus atoms per layer. On each face of the cells, the periodic boundary conditions were applied. To prevent undesirable interaction with atom images, a 25 A void buffer was added at the top of the slab. The cell of a single layer structure along with strained slabs are displayed in **Figure 1A.1 and 1A.1**. After geometry optimisation, structures with the geometrical properties presented in **Table 1** were achieved.

Table 1. Basic geometric and mechanical properties of phosphorene cell model used in experiments compared with experimental and *ab-initio* values.

	a [Å]	b [Å]	c [Å]	σ armchair	σ zigzag	E armchair [GPa]	E zigzag [GPa]
Experimental [37]	3.31	5.4	4.34	-	-	-	-
Calculated [13]	3.30	-	4.62	0.175	0.703	23.0	92.3
Calculated [14]	3.299	5.5	4.643	-	-	34.4	164.9
Calculated by authors	3.31	5.38	4.11	0.1984	1.009	32.5	143.9

According to the data presented in **Table 1**, the simulated geometry dimensions of the phosphorene structure do not differ much between each other as from the experimental results. The mechanical properties are much more challenging. There is a significant lack of reliable experimental data about the properties such as the Young Modulus, and Poisson's ratio. On the other hand, there are many *ab-initio* studies for such properties [13,14,38]. According to existing data, phosphorene exhibits strong anisotropic and nonlinear mechanical properties, especially for high strains (over 20%). At approximately 20% strain, the Poisson ratio became negative according to theoretical calculations [39]. This feature can be observed only on the armchair direction because the zigzag critical strain is lower than 20%. Unfortunately, the achieved results vary between each other, as can be seen in **Table 1**. A remarkable, reported fact is that the Young modulus is different for small and for large strains [14].

2.2. Vibrational properties of the structure

A single cell of phosphorene structure was considered in the paper. There are a total of 12 vibrational modes possible in such a structure. Three belong to the acoustic branch, and nine to optical [11]. Six of them are reported to be Raman active [11,21,26]. In this study, the focus

was put on the three vibrational modes presented in **Figure 1B**. The corresponding Raman shifts of these modes are 360, 440, and 468 cm^{-1}, respectively [23]. Other author performing Raman measurements on plasma-treated phosphorene set the energies of these modes on 363, 440 and 470 cm^{-1}, respectively [24]. The side sub-bands observed at higher strains could be attributed to the second-order symmetric Raman scattering modes identified by Favron at al. [40]. They are positioned close to the bulk A^1_g and A^2_g modes for layered BP and induced by intra-valley scattering along the armchair and zigzag directions.

The estimated rate of shift for A^1_g peak observed in the armchair direction reaches 1.879 cm^{-1}/% , which is corresponding to the 1.47 cm^{-1}/GPa induced by the pressure in the Raman studies conducted by Akhtar at al. [23].

In the present work, the focus was put on the dependence of the phonon density of states (PDOS) on the strain applied to the structure. **Figure 2** illustrates the series of single-layer black phosphorus PDOS depending on the applied strain. The positions of the modes presented in **Figure 2** are marked and attributed to the specific vibration as listed in the legend.
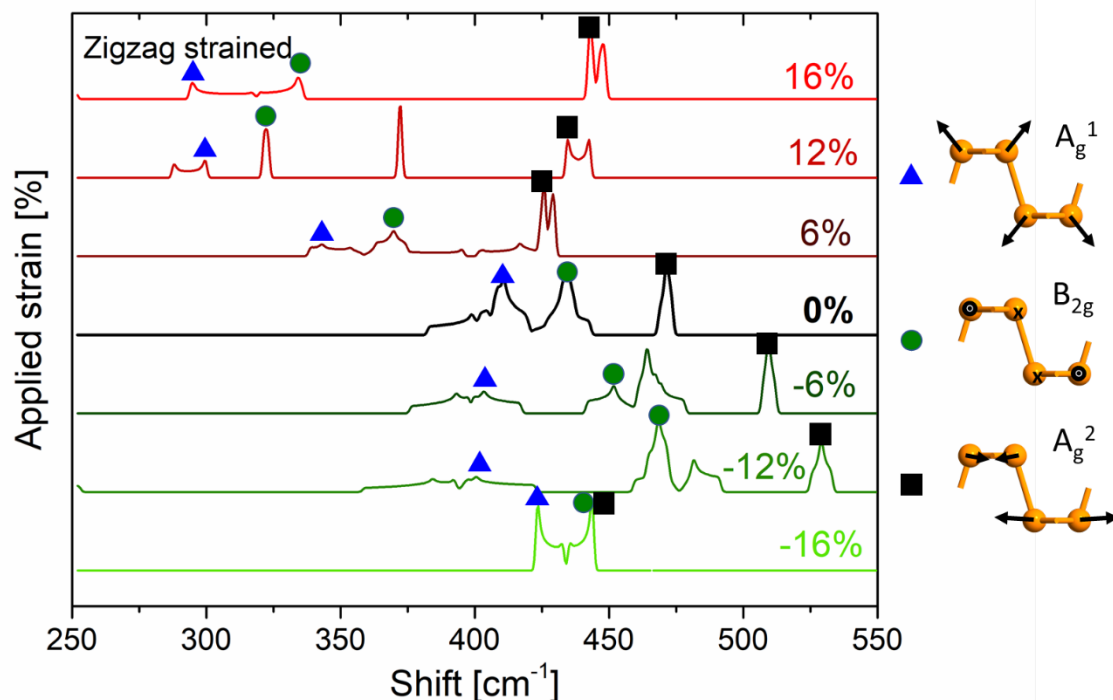

Figure 2. Distribution of PDOS and vibrational modes for strains along the zigzag axis, single layer structure.

In the rest of the paper, notation consistent with [41] will be used, so if the vibration mode energy increases, this will be called blue shift, and if it decreases, red shift.

To show how the changes in the positions of the peaks depend on changes in the structure geometry caused by strain, another plot was created **(Figure 3)**. **Figure 3b** shows the dependence of the positions of the PDOS peaks connected with the analysed vibrational modes on the applied strain in a similar way to **Figure 2**. The dependence of the bond length versus the applied strain is presented in **Figure 3a** as labelled in inset. The strain effect on the vibration mode energy change considers the behaviour of the bonded structure of BP. The vibrations associated with the B_{2g} and A_g^2 modes were induced in the plane of structure. After the application of strain in the zigzag direction of the phosphorene structure, a significant portion of the strain is provided by the stretching of bonds 1 and 3 (see **Figure 1A.1**). Qualitatively, the relative change in length for both the 1 and 2 bonds is equal to 40% of the relative change in the length of the cell, which is visible in **Figure 3a**. In contrast, the similar parameter for bond number 2 is 8%. As a result, the energy of the bonds decreases, which lowers the force constant for atomic oscillation, and consequently decreases the energy of the oscillations, as can be observed in **Figure 3b**.
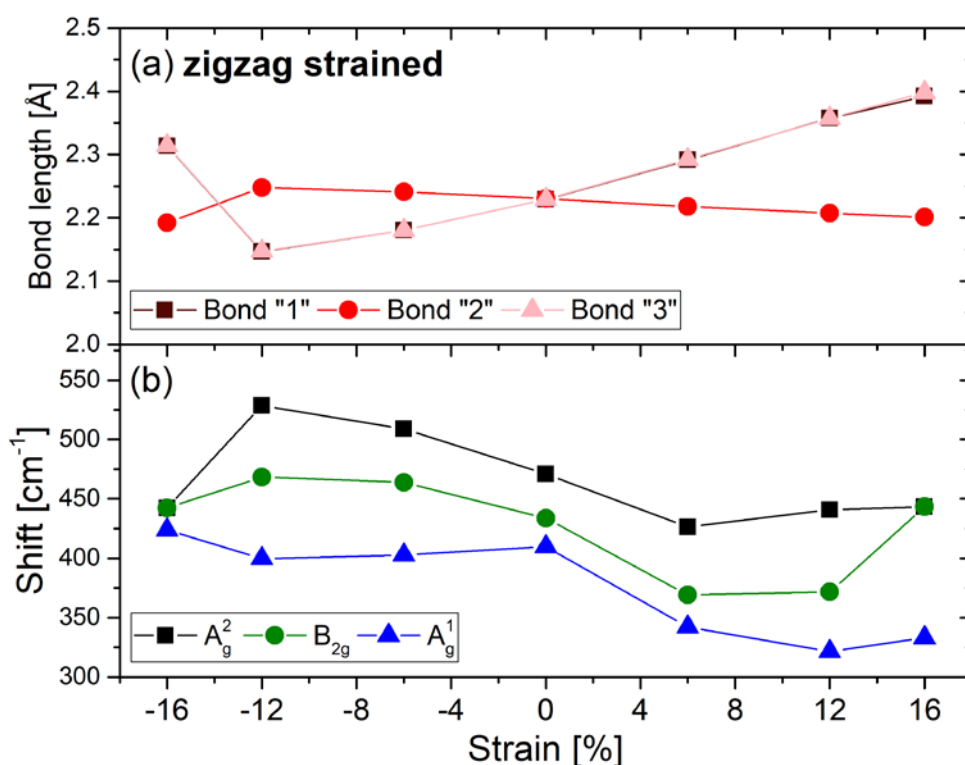

Figure 3. The variations of bond length changes with strain applied in the zigzag direction (a) and dependence of selected peaks' positions on the strain applied on the zigzag axis (b).

Generally, the shift of peaks in the PDOS of black phosphorene under strain applied in the zigzag direction is monotonic for small strains of peaks corresponding to modes B_{2g} and A_g^2.

In the framework of the presented simulations, all modes exhibited red shifts for the zigzag strains. The quantity values of these shift rates are presented in the **Table 2**.

Table 2. The rates of shift for PDOS peaks. The rates were estimated for small strains from -5 to 5 %.

Mode	Armchair direction [cm^{-1}/%]	Zigzag direction [cm^{-1}/%]
A^1_g	1.879	-5.052
B_{2g}	3.424	-7.891
A^2_g	1.503	-6.889

For strains applied over the armchair direction, the blue shift is dominant, especially for negative strains. For positive strains, the rate became negatively red, but as pointed out in **Table 2**, the mean rate for small strains is blue.
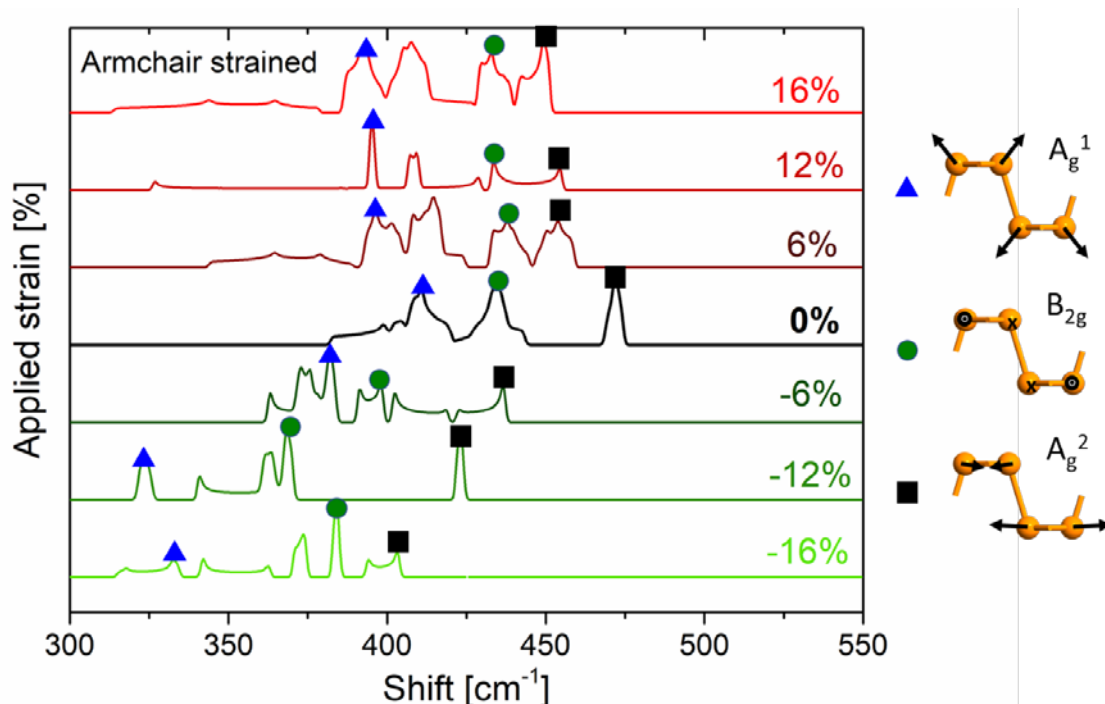

Figure 4. Distribution of PDOS and vibrational modes for strains along the armchair axis, single layer structure.

This is generally consistent with the experimental data presented in [20]. The main difference refers to the A^1_g mode. This mode is a breathing mode, as the atoms move perpendicular to the plane. In contrast, B_{2g} and A^2_g modes are shear modes, where the atoms move mainly in plane.

Thus, A^1_g is much more sensitive to the presence of the other layers of the structure. The mentioned experimental results refer to few-layer phosphorene because of technical problems with single-layer phosphorene. This presence of additional layers of the structure is the reason for the changes in the behaviour of the A^1_g mode.

The peaks' shifts tend to become higher when the strain increases (see **Figure 4**). This dependence is not monotonic, and is clearly more rapid for compressing strain. Moreover, the peaks' shifts lower more for armchair strain than for zigzag strain. This phenomenon is clearly connected with phosphorene anisotropy. Similarly, to what was done for the zigzag direction, the analyses of this case for bond length were conducted. **Figure 4b** presents the peaks' shifts caused by applied strain and bound length changes. One can note that the direction of changes in bond length are reversed, which remains consistent with the previous considerations. For compressive and for small tensile strains, the changes in bonds 1 and 3 are dominant (see **Figure 4a**). At about 5% strain, their dynamics decrease by an order of magnitude. Qualitatively, the relative change in lengths for both bonds 1 and 2 equal 13% of the relative change in the length of the cell for strains under 5%, and above this limit, they decrease to a value of about 1%. Similarly, the change in bond number 2 increases at 6 % strain from 1% to 13 %.
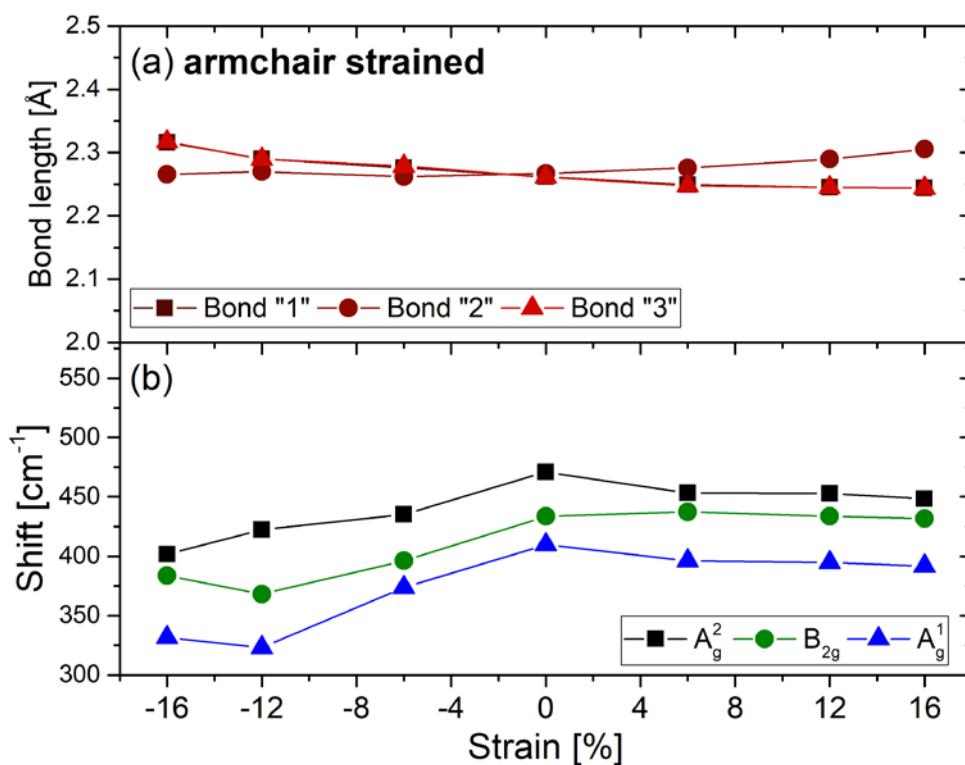

Figure 5. The variations of bond length changes with strain applied in the armchair direction (a) and dependence of selected peaks' positions on the strain applied on the armchair axis (b).

Generally, the bond length changes are much smaller for armchair strains than for zigzag strain. The Young modulus is significantly higher along the zigzag direction than for the armchair direction (see **Table 1**), so this conclusion is consistent with the macroscopic effects occurring in phosphorene.

The vibrational modes exhibit a similar reaction to the applied armchair strain. While the changes in the lengths of bonds 1 and 3 slow down at a strain of about 6%, the changes in A_g^1, B_{2g}, and A_g^2 slow down too, by an order of magnitude. This case clearly shows that even for mode A_g^1, the most important portion of the energy is determined by the force constant of bonds 1 and 3.

3. Conclusions

In presented work, the *ab-initio* simulation of the influence of strain on the PDOS and vibrational modes of phosphorene were investigated. The set of phosphorene vibrational modes was tuned by the applied strain. An analysis of changes in bond length was conducted, providing important information about the explanations of variation in the modes' energy. The data revealed by the calculations allowed for the following conclusions:

- The response of the phosphorene vibrational spectrum for a high strain (above 5%) is anisotropic. It was shown that the response to the external pressure applied in the zigzag direction is different from the response to the pressure applied in the armchair direction. This is consistent with previous experimental studies focused on Raman spectroscopy.

- The rates of shift of modes B_g^2 and A_g^2 for minor strains are positive for the armchair direction and negative for zigzag. This is consistent with experimental results [20], and with simulations conducted using other methods [21,42]. The main difference concerns the A_g^1 mode shift rate. This difference could be explained by this study being limited to single-layer phosphorene, while the experimental results refers to few-layer structures [43].

- The behaviour of the vibrational spectrum of phosphorene can be explained by an analysis of covalent bond length changes. It was shown that blue shifts are connected with shortening of specific bonds while the red shifts are attributed to the extending of the length of these bonds.

- A negative Poison ratio was manifested in phosphorene for large strains (above 20%), and on direction transverse to its planes. Thus, the negative values of the Poisson ratio reported in phosphorene [39,43] was not observed here.

A crucial point was to investigate the position of the important Raman active modes as a function of applied strain. The binding of the "light weight" LCAO algorithm with the Wigner-Seitz scheme for the calculation of the dynamical matrix, allowed for an efficient cost of such a calculation to be achieved. This approach is suitable for studying the vibrational properties of much more complex structures, including defected phosphorene flakes and nanoribbons.

Acknowledgements

Bibliography

[1]   A. Carvalho, M. Wang, X. Zhu, A.S. Rodin, H. Su, A.H. Castro Neto, Phosphorene: From theory to applications, Nat. Rev. Mater. 1 (2016). https://doi.org/10.1038/natrevmats.2016.61.

[2]   T.-D. Chou, T.-W. Lee, S.-L. Chen, Y.-M. Tung, N.-T. Dai, S.-G. Chen, C.-H. Lee, T.-M. Chen, H.-J. Wang, The management of white phosphorus burns, Burns. 27 (2001) 492–497. https://doi.org/10.1016/S0305-4179(01)00003-1.

[3]   L. Kou, C. Chen, S.C. Smith, Phosphorene: Fabrication, Properties, and Applications, J. Phys. Chem. Lett. 6 (2015) 2794–2805. https://doi.org/10.1021/acs.jpclett.5b01094.

[4]   E.S. Reich, others, Phosphorene excites materials scientists, Nature. 506 (2014) 19.

[5]   R. Mas-Ballesté, C. Gómez-Navarro, J. Gómez-Herrero, F.F.F. Zamora, R. Mas-Balleste, C. Gomez-Navarro, J. Gomez-Herrero, F.F.F. Zamora, R. Mas-Ballesté, C. Gómez-Navarro, J. Gómez-Herrero, F.F.F. Zamora, 2D materials: to graphene and beyond, Nanoscale. 3 (2011) 20–30. https://doi.org/10.1039/c0nr00323a.

[6]   Y. Ding, Y. Wang, Structural, electronic, and magnetic properties of adatom adsorptions on black and blue phosphorene:A first-Principles study, J. Phys. Chem. C. 119 (2015) 10610–10622. https://doi.org/10.1021/jp5114152.

[7]   D.W. Boukhvalov, A.N. Rudenko, D.A. Prishchenko, V.G. Mazurenko, M.I. Katsnelson, Chemical modifications and stability of phosphorene with impurities: A first principles study, Phys. Chem. Chem. Phys. 17 (2015) 15209–15217. https://doi.org/10.1039/c5cp01901j.

[8]   Y. He, S. Xiong, F. Xia, Z. Shao, J. Zhao, X. Zhang, J. Jie, X. Zhang, Tuning the

electronic transport anisotropy in α -phase phosphorene through superlattice design, Phys. Rev. B. 97 (2018) 1–10. https://doi.org/10.1103/PhysRevB.97.085119.

[9]   S. Fukuoka, T. Taen, T. Osada, Electronic Structure and the Properties of Phosphorene and Few-Layer Black Phosphorus, J. Phys. Soc. Japan. 84 (2015) 121004. https://doi.org/10.7566/JPSJ.84.121004.

[10] R. Fei, L. Yang, Strain-Engineering the Anisotropic Electrical Conductance of Few-Layer Black Phosphorus, Nano Lett. 14 (2014) 2884–2889. https://doi.org/10.1021/nl500935z.

[11] Y. Cai, Q. Ke, G. Zhang, Y.P. Feng, V.B. Shenoy, Y.W. Zhang, Giant phononic anisotropy and unusual anharmonicity of phosphorene: Interlayer coupling and strain engineering, Adv. Funct. Mater. 25 (2015) 2230–2236. https://doi.org/10.1002/adfm.201404294.

[12] Z. Jin, J.T. Mullen, K.W. Kim, Highly anisotropic electronic transport properties of monolayer and bilayer phosphorene from first principles, Appl. Phys. Lett. 109 (2016) 053108. https://doi.org/10.1063/1.4960526.

[13] L. Wang, A. Kutana, X. Zou, B.I. Yakobson, Electro-mechanical anisotropy of phosphorene, Nanoscale. 7 (2015) 9746–9751. https://doi.org/10.1039/c5nr00355e.

[14] W. Zhang, J. Yin, P. Zhang, Y. Ding, Strain/stress engineering on the mechanical and electronic properties of phosphorene nanosheets and nanotubes, RSC Adv. 7 (2017) 51466–51474. https://doi.org/10.1039/c7ra09668b.

[15] M. Elahi, K. Khaliji, S.M. Tabatabaei, M. Pourfath, R. Asgari, Modulation of electronic and mechanical properties of phosphorene through strain, Phys. Rev. B - Condens. Matter Mater. Phys. 91 (2015). https://doi.org/10.1103/PhysRevB.91.115412.

[16] H. V. Phuc, N.N. Hieu, V. V. Ilyasov, L.T.T. Phuong, C. V. Nguyen, First principles study of the electronic properties and band gap modulation of two-dimensional phosphorene monolayer: Effect of strain engineering, Superlattices Microstruct. 118 (2018) 289–297. https://doi.org/10.1016/j.spmi.2018.04.018.

[17] A. Manjanath, A. Samanta, T. Pandey, A.K. Singh, Semiconductor to metal transition in bilayer phosphorene under normal compressive strain, Nanotechnology. 26 (2015) 75701. https://doi.org/10.1088/0957-4484/26/7/075701.

[18] D.Q. Khoa, M. Davoudiniya, B.D. Hoi, M. Yarmohammadi, Strain engineering of optical activity in phosphorene, RSC Adv. 9 (2019) 19006–19015. https://doi.org/10.1039/c9ra03696b.

[19] P. Tan, Correction to: Raman Spectroscopy of Two-Dimensional Materials, in: 2019: pp. C1–C1. https://doi.org/10.1007/978-981-13-1828-3_12.

[20] W. Zhu, L. Liang, R.H. Roberts, J.F. Lin, D. Akinwande, Anisotropic Electron-Phonon Interactions in Angle-Resolved Raman Study of Strained Black Phosphorus, ACS Nano. 12 (2018) 12512–12522. https://doi.org/10.1021/acsnano.8b06940.

[21] R. Fei, L. Yang, Lattice vibrational modes and Raman scattering spectra of strained phosphorene, Appl. Phys. Lett. 105 (2014). https://doi.org/10.1063/1.4894273.

[22] Y. Feng, J. Zhou, Y. Du, F. Miao, C.G. Duan, B. Wang, X. Wan, Raman spectra of few-layer phosphorene studied from first-principles calculations, J. Phys. Condens. Matter.

27 (2015). https://doi.org/10.1088/0953-8984/27/18/185302.

[23] M. Akhtar, C. Zhang, M. Rajapakse, M.R.K. Musa, M. Yu, G. Sumanasekera, J.B. Jasinski, Bilayer phosphorene under high pressure:: In situ Raman spectroscopy, Phys. Chem. Chem. Phys. 21 (2019) 7298–7304. https://doi.org/10.1039/c9cp00816k.

[24] W. Lu, H. Nan, J. Hong, Y. Chen, C. Zhu, Z. Liang, X. Ma, Z. Ni, C. Jin, Z. Zhang, Plasma-assisted fabrication of monolayer phosphorene and its Raman characterization, Nano Res. 7 (2014) 853–859. https://doi.org/10.1007/s12274-014-0446-7.

[25] M. Akhtar, G. Anderson, R. Zhao, A. Alruqi, J.E. Mroczkowska, G. Sumanasekera, J.B. Jasinski, Recent advances in synthesis, properties, and applications of phosphorene, Npj 2D Mater. Appl. 1 (2017) 1–12. https://doi.org/10.1038/s41699-017-0007-5.

[26] Z. Deng, Z. Li, W. Wang, J. She, Vibrational properties and Raman spectra of pristine and fluorinated blue phosphorene, Phys. Chem. Chem. Phys. 21 (2019) 1059–1066. https://doi.org/10.1039/c8cp05699d.

[27] Y.Y. Sun, S. Zhang, Communication: Effect of accidental mode degeneracy on Raman intensity in 2D materials: Hybrid functional study of bilayer phosphorene, J. Chem. Phys. 145 (2016) 1–5. https://doi.org/10.1063/1.4958460.

[28] R.A. Evarestov, E. Blokhin, D. Gryaznov, E.A. Kotomin, J. Maier, Phonon calculations in cubic and tetragonal phases of SrTiO3: A comparative LCAO and plane-wave study, Phys. Rev. B - Condens. Matter Mater. Phys. 83 (2011) 1–9. https://doi.org/10.1103/PhysRevB.83.134108.

[29] S. Smidstrup, D. Stradi, J. Wellendorff, P.A. Khomyakov, U.G. Vej-Hansen, M.-E. Lee, T. Ghosh, E. Jónsson, H. Jónsson, K. Stokbro, First-principles Green's-function method for surface calculations: A pseudopotential localized basis set approach, Phys. Rev. B. 96 (2017) 195309. https://doi.org/10.1103/PhysRevB.96.195309.

[30] R.M.A. Khalil, J. Ahmad, A.M. Rana, S.H. Bukhari, M. Tufiq Jamil, T. Tehreem, U. Nissar, First principles investigation of structural, vibrational and thermal properties of black and blue phosphorene, Int. J. Mod. Phys. B. 32 (2018) 1–8. https://doi.org/10.1142/S0217979218501515.

[31] B. Mortazavi, T. Rabczuk, Anisotropic mechanical properties and strain tuneable band-gap in single-layer SiP, SiAs, GeP and GeAs, Phys. E Low-Dimensional Syst. Nanostructures. 103 (2018) 273–278. https://doi.org/10.1016/j.physe.2018.06.011.

[32] Atomistix Toolkit version 2019.03, Synopsys QuantumWise A/S (www.quantumwise.com)., (n.d.).

[33] Jos, M. Soler, A. Emilio, D.G. Julian, G. Alberto, J. Javier, O. Pablo, S. Daniel, P. Nchez, The SIESTA method for ab initio order-N materials simulation, J. Phys. Condens. Matter. (2002) 2745. https://doi.org/10.1088/0953-8984/14/11/302.

[34] M. Schlipf, F. Gygi, Optimization algorithm for the generation of ONCV pseudopotentials, Comput. Phys. Commun. 196 (2015) 36–44. https://doi.org/10.1016/j.cpc.2015.05.011.

[35] S. Grimme, J. Antony, S. Ehrlich, H. Krieg, A consistent and accurate ab initio parametrization of density functional dispersion correction (DFT-D) for the 94 elements H-Pu, J. Chem. Phys. 132 (2010). https://doi.org/10.1063/1.3382344.

[36] P.E. Blöchl, O. Jepsen, O.K. Andersen, Improved tetrahedron method for Brillouin-zone integrations, Phys. Rev. B. 49 (1994) 16223–16233. https://doi.org/10.1103/PhysRevB.49.16223.

[37] R.J. Wu, M. Topsakal, T. Low, M.C. Robbins, N. Haratipour, J.S. Jeong, R.M. Wentzcovitch, S.J. Koester, K.A. Mkhoyan, Atomic and electronic structure of exfoliated black phosphorus, J. Vac. Sci. Technol. A Vacuum, Surfaces, Film. 33 (2015) 060604. https://doi.org/10.1116/1.4926753.

[38] J.W. Jiang, T. Rabczuk, H.S. Park, A Stillinger-Weber potential for single-layered black phosphorus, and the importance of cross-pucker interactions for a negative Poisson's ratio and edge stress-induced bending, Nanoscale. 7 (2015) 6059–6068. https://doi.org/10.1039/c4nr07341j.

[39] H. Wang, X. Li, P. Li, J. Yang, δ-Phosphorene: A two dimensional material with a highly negative Poisson's ratio, Nanoscale. 9 (2017) 850–855. https://doi.org/10.1039/c6nr08550d.

[40] A. Favron, F.A. Goudreault, V. Gosselin, J. Groulx, M. Côté, R. Leonelli, J.F. Germain, A.L. Phaneuf-L'Heureux, S. Francoeur, R. Martel, Second-Order Raman Scattering in Exfoliated Black Phosphorus, Nano Lett. 18 (2018) 1018–1027. https://doi.org/10.1021/acs.nanolett.7b04486.

[41] S. Zhang, J. Yang, R. Xu, F. Wang, W. Li, M. Ghufran, Y.-W. Zhang, Z. Yu, G. Zhang, Q. Qin, Y. Lu, Extraordinary Photoluminescence and Strong Temperature/Angle-Dependent Raman Responses in Few-Layer Phosphorene, ACS Nano. 8 (2014) 9590–9596. https://doi.org/10.1021/nn503893j.

[42] K. Tokár, R. Derian, J. Brndiar, I. Štich, Strain control of vibrational properties of few layer phosphorene, J. Appl. Phys. 120 (2016) 1–17. https://doi.org/10.1063/1.4968009.

[43] Y. Du, J. Maassen, W. Wu, Z. Luo, X. Xu, P.D. Ye, Auxetic Black Phosphorus: A 2D Material with Negative Poisson's Ratio, Nano Lett. 16 (2016) 6701–6708. https://doi.org/10.1021/acs.nanolett.6b03607.